Inhomogeneities in acid-catalyzed titania–silica and zirconia–silica xerogels as revealed by small-angle x-ray scattering

G. Mountjoy, J.S. Rigden, and R. Anderson
School of Physical Sciences, University of Kent at Canterbury, Canterbury CT2 7NR, United Kingdom
G.W. Wallidge
Department of Physics, University of Warwick, Coventry CV4 7AL, United Kingdom
R.J. Newport
School of Physical Sciences, University of Kent at Canterbury, Canterbury CT2 7NR, United Kingdom
M.E. Smith
Department of Physics, University of Warwick, Coventry CV4 7AL, United Kingdom

(Received 24 January 2000; accepted 23 June 2000)

The small-angle x-ray scattering (SAXS) technique was used to investigate inhomogeneities on the scale of 10 to 600 Å in acid-catalyzed titania–silica and zirconia–silica xerogels. SAXS of $(TiO_2)_x(SiO_2)_{1-x}$ and $(ZrO_2)_x(SiO_2)_{1-x}$ xerogels with $x < 0.1$, in which there was no phase separation, showed the presence of two types of inhomogeneity. For $Q < 0.05$ Å^{-1} there was a clear departure from Porod scattering which showed that xerogel powder particle surfaces were rough. For $0.1 < Q < 0.4$ Å^{-1} there was a plateau feature corresponding to micropores within the silica-based network, and this feature changes with heat treatment. SAXS of xerogels with $x > 0.3$ showed the presence of phase-separated regions of metal oxide, which were initially amorphous and crystallized at higher temperatures. A $(TiO_2)_{0.18}(SiO_2)_{0.82}$ xerogel that was not initially phase separated became phase separated after heat treatment at 750 °C due to reduced solubility of Ti in the silica network.

I. INTRODUCTION

Mixed titania–silica materials, $(TiO_2)_x(SiO_2)_{1-x}$, are useful in a number of technological applications,[1] such as ultralow expansion glasses, antireflective thin film coatings, and catalytic materials.[2] Mixed zirconia–silica materials, $(ZrO_2)_x(SiO_2)_{1-x}$, have low thermal expansion, tunable refractive index, and high physical and chemical durability[3] and have potentially useful catalytic properties.[4] However, the preparation of these mixed oxide materials by high-temperature methods is difficult because of the high melting temperatures involved.

The sol-gel process[5] has the advantages of using liquid precursors and involving relatively low processing temperatures. A sol of water and metal alkoxide(s) undergoes hydrolysis and condensation reactions to produce a gel. A gel is dried to produce a xerogel, generally an amorphous, porous, hydrated solid. This becomes similar to a melt-quenced glass during heat treatment (up to ~1000 °C). The structures of xerogels are strongly dependent on the details of preparation and heat treatment. For example, base-catalyzed gels have a colloidal structure, whereas acid-catalyzed gels have a polymeric structure.[5] Furthermore, conventionally aged/dried acid-catalyzed gels, i.e., xerogels, are microporous, whereas mesoporous structures called aerogels can be produced by using special aging/drying conditions.

The degree of homogeneity in xerogels is an important issue for investigation. Acid-catalyzed xerogels are commonly prepared with two-step hydrolysis and low water: alkoxide ratio, i.e., $1 \leq R_w \leq 5$, to promote homogeneity. Titania– and zirconia–silica xerogels prepared in this way are the subject of the present study. They have previously been investigated using diffraction,[6–9] ultraviolet,[10] infrared,[10–13] nuclear magnetic resonance (NMR),[11,12,14] and x-ray absorption spectroscopies.[8,11,15–17] In particular, our group has studied the same sets of samples using several of these techniques.[6,7,11,14–16] Generally, metal atoms are homogeneously incorporated into the silica network at low concentrations, i.e., $x < 0.2$, and separation of a metal oxide phase begins to occur at higher concentrations. However, details of atomic structure provide only a partial description of these materials.

Acid-catalyzed titania–silica and zirconia–silica xerogels have intrinsic inhomogeneities beyond atomic length scales.[5] Gelation creates an undercondensed polymer network, drying modifies the network and exposes

pores, and heat treatment causes shrinkage of the network and possibly separation of a metal oxide phase. A better understanding of porosity and phase separation will assist efforts to use these materials in catalytic applications,[2,4] which depend on accessible surface area and distribution of metal atom sites.

Small-angle scattering,[18] with scattering angle θ, is sensitive to inhomogeneities on large length scales λ/θ (where λ is the wavelength of the scattered particle). There have previously been only a few reports of small-angle scattering on samples of the kind studied here. Small-angle neutron scattering (SANS) has been applied to titania[19] and zirconia–silica,[20] sols and xerogels. Small-angle x-ray scattering (SAXS) has been applied to silica,[21] titania–silica,[22] and zirconia–silica[23] sols. Here we apply SAXS to the same xerogel samples previously studied using atomic structural methods.[6,7,11,14–16] We present measurements of the SAXS scattering intensity over angular ranges corresponding to length scales from 10 to 600 Å and interpret the observed features in terms of the known structural features of these materials.[5]

II. METHOD

A. Sample preparation

The $(TiO_2)_x(SiO_2)_{1-x}$ samples were prepared using a two-step hydrolysis procedure.[24] In the first step, tetraethoxyorthosilicate (TEOS) was mixed with water and 2-propanol as solvent in approximately equimolar ratios, with an HCl catalyst of pH = 1. After 2 h, Ti isopropoxide, and then water, were added dropwise while stirring, such that the final ratio of alkoxide to water, R_w, equals 2. With this ratio, complete condensation occurs by utilizing all of the water released during hydrolysis. The $(TiO_2)_x(SiO_2)_{1-x}$ samples were prepared in the same way, except that the solvent was propan-1-ol and the metal alkoxide was Zr *n*-propoxide diluted 1:5 in propan-1-ol. The $(TiO_2)_x(SiO_2)_{1-x}$ samples had $x = 0.08$, 0.18, and 0.41. Pure SiO_2 samples were also prepared in this way. The $(ZrO_2)_x(SiO_2)_{1-x}$ samples had $x = 0.07$, 0.23, and 0.32. The sols were aged to produce gels. The gels were dried under ambient conditions, and then under vacuum, to produce xerogels. Xerogel samples taken from a common feedstock were subjected to different heat treatments consisting of heating at 5 °C/min followed by 2 h at constant temperature in air.

In the SAXS experiments, both sol and xerogel samples were examined. The xerogel samples were prepared prior to the experiment, according to the procedure described above. The sol samples were prepared during the experiment, also according to the procedure described above. However, they were then aged *in situ*. Hence the aging conditions were not identical to those for the xerogel samples. Furthermore, the *in situ* aging was difficult to control, and only sol samples with $x < 0.1$ were examined.

B. Theory of small-angle scattering

Features in SAXS intensity, $I(Q)$, arise because a sample contains inhomogeneities in the spatial distribution of electron density,[18] which we equate with mass denisty as both depend on average atomic number Z. The angular scale of scattering is described by $Q = 4\pi\sin(\theta/2)/\lambda \approx 2\pi\theta/\lambda$. As in diffraction, $I(Q)$ can be interpreted as the product of a form factor representing the scattering from individual objects and a structure factor representing spatial correlations between objects. However, this formalism is not always tractable in SAXS because of ambiguities in the interpretation of inhomogeneities in density over large length scales (10 to 600 Å in the experiments presented here). Hence approximations are useful for interpreting SAXS features.

Sol samples are liquids containing random density fluctuations due to the partial polymerisation of alkoxides. Such inhomogeneity can be modeled using the Ornstein–Zernike equation,[18]

$$I(Q) = \frac{I_0}{(1 + \xi^2 Q^2)} \quad , \tag{1}$$

where ξ is the correlation length, or characteristic length scale of fluctuations. Models of this kind have previously been applied to acid-catalyzed sols.[19,21,22] However, the model is not valid once gelling begins to occur, because then fluctuations become constrained due to the space-filling nature of the polymer network.

Xerogel samples are powdered and typically have packing densities of 50%. For such samples, the inhomogeneities at largest length scales are due to powder particles and interparticle voids [see Fig. 1(a)]. For values of Q^{-1} which are much smaller than the typical particle size (~μm), but much larger than typical inhomogeneities within a particle (~nm), the scattering contrast is due to particle surfaces. For smooth, sharp surfaces the scattering is described by the Porod equation,[18]

$$I(Q) = I_0 Q^{-n} \quad , \tag{2}$$

with $n = 4$. This result is not valid for rough surfaces. For surface roughness in the form of a surface fractal it is found that $n = 6 - d_s < 4$, where $d_s > 2$ is the surface fractal dimension.[25] An equivalent result is obtained for surface roughness in the form of self-affine surfaces.[26]

Inhomogeneities within xerogel particles arise for at least two reasons. First, acid-catalyzed xerogels are microporous,[5] and on length scales ≤2 nm there is contrast between the homogenous silica-based network and pores [see Figure 1(b)]. This is not simple to describe as the

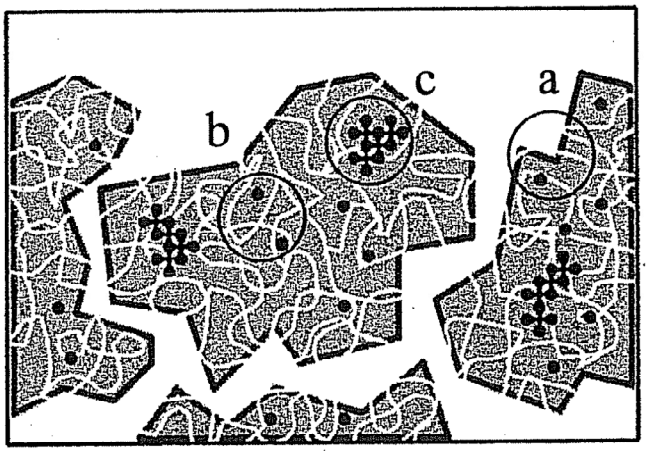

FIG. 1. Inhomogeneities in acid-catalyzed silica-based xerogel powders: (a) rough particle surfaces (due to micropore permeation and fracture), (b) micropores which permeate the silica-based network (the latter includes homogeneously mixed metal atoms), and (c) regions of phase-separated metal oxide.

pore network is extensive and is formed by complex processes during aging and drying of the gel. However, the length scales of inhomogeneities due to micropores are much smaller than those due to particle surfaces, Second, mixed titania– and zirconia–silica xerogels may contain regions of phase separated metal oxide [see Fig. 1(c)] (e.g., Refs. 11 and 16). For $QR_G < 1$, the scattering from independent regions of finite spatial extent can be approximated using the Guinier equation.[18]

$$I(Q) = I_0 \exp(-R_G^2 Q^2/3) \quad , \qquad (3)$$

where R_G is the radius of gyration ($R_G = 0.77 \times$ radius for a solid sphere). Note that the length scales of inhomogeneities due to phase separation overlap with those due to particle surfaces and micropores.

C. Experiment

The SAXS experiments were carried out on station 8.2 of the SRS, Daresbury Laboratory, Warrington, U.K. X-rays of wavelength $\lambda = 1.54$ Å were used, with four sets of collimating slits to reduce slit scattering. Incident and transmitted x-ray intensities, I_i and I_t, were measured using standard ion chambers before and after the sample (respectively). Samples were contained in cells between two thin sheets kapton or mica. The empty container scattering was also measured.

The SAXS intensity was recorded using a quadrant detector. The SAXS detector response was calibrated periodically using a radioactive ^{55}Fe source. The angular scale for SAXS is determined by the distance from sample to the detector, or camera length, L, and the size of the detector elements, d, where $\theta_n \approx nd/L$ for the nth detector element. The angular scale for SAXS was calibrated from a reference sample of wet rat's tail collagen. The first, preliminary experiment used a camera length of 1.5 m with approximate Q-range of 0.03 to 0.6 Å^{-1}. The second, more detailed experiment used a camera length of 3.5 m with approximate Q-range of 0.01 to 0.2 Å^{-1}.

For slits of finite size, s, the distance from sample to detector varies from L to $(L^2 + s^2)^{0.5}$. This effect, known as slit-smearing,[27] reduces the Q-resolution in $I(Q)$ at low Q. Slit-smearing was simulated[27] and was found to be non-negligible for $Q < 0.05$ Å^{-1}. When $I(Q)$ has a strong Q-dependence at low Q, for example Q^{-n} due to the surfaces of powder particles (see Sec. II. B), slit-smearing causes the measured value of n to be less than the expected value. This effect can be calibrated by measuring $I(Q)$ for reference samples of nonporous powders with smooth surfaces, such as fused silica and NaCl. For camera lengths of 1.5 and 3.5 m the calibration gave measured $n = 3.0 \pm 0.1$ and 3.65 ± 0.05 (respectively) compared with expected $n = 4.0$ for Porod scattering from smooth surfaces. The effect of slit-smearing is much greater for the shorter camera length.[27]

During the SAXS experiments, conventional diffraction, or wide-angle x-ray scattering (WAXS), was simultaneously recorded using a curved INEL detector (Artenay, France). The angular scale for WAXS was calibrated from a reference sample of high density polyethylene. The Q-range was 0.8 to 5.6 Å^{-1}, corresponding to d-spacings from 1.2 to 7.2 Å.

D. Data reduction

The raw data are divided by the detector response function and normalized to incident beam current and counting time. The absorption correction is simplified by using the approximation $\theta \approx 0$, i.e., no path length variation. In this case, the scattering intensity including absorption, $I'(Q)$, is given by

$$I'(Q)_{sc} = I(Q)_s \exp(-\mu_c t_c - \mu_s t_s) + I(Q)_c \exp(-\mu_c t_c - \mu_s t_s)$$
$$= (I(Q)_s + I(Q)_c)(I_t/I_i)_{sc} \quad , \qquad (4)$$

where $I(Q)$ is the scattering intensity without absorption, μ is the linear absorption coefficient, t is thickness, "SC" denotes sample plus container, and "C" denotes container only. Hence the scattering intensity from sample corrected for container and absorption is

$$I(Q)_S = I'(Q)_{SC}(I_i/I_t)_{SC} - I'(Q)_C(I_i/I_t)_C \quad . \qquad (5)$$

An approximate correction for variations in sample thickness was made by multiplying $I(Q)_S$ by the factor $(\mu_S t_S)^{-1}$. No reduction of the WAXS data was carried out, as the raw data were sufficient for observing the Bragg peaks indicative of crystallization.

III. RESULTS

A. TiO_2–SiO_2 and ZrO_2–SiO_2 sols

Figure 2 shows $I(Q)$ measured *in situ* during the aging of (a) $(TiO_2)_{0.08}(SiO_2)_{0.92}$ and (b) $(ZrO_2)_{0.07}(SiO_2)_{0.93}$ sols. Three representative results are shown during a total

aging time of ~12 h. The full set of $I(Q)$ data have been fitted using the Ornstein–Zernike equation [Eq. (1)], and the results are presented in Fig. 3. Due to the difficulty of controlling *in situ* gelling, only two results were obtained for gels. Figures 2(c) and 2(d) show $I(Q)$ for two $(ZrO_2)_{0.07}(SiO_2)_{0.93}$ gels which are in the initial drying phase. These gels were formed from sols which were initially aged for 12 h and then heated at 50 °C for (c) 4 h and (d) 12 h. During aging, the structure of a gel changes due to evaporation from the surface, expulsion of liquid from spaces within the polymer network, and consolidation of the network.[5] During drying there is continued evaporation which results in the exposure of micropores.[5] The $I(Q)$ for the gels [see Figs. 2(c) and 2(d)] are clearly intermediate between those for the sols [see Fig. 2(b)] and xerogels (see Sec. III. D). A similar $I(Q)$ was reported for a $(ZrO_2)_{0.3}(SiO_2)_{0.7}$ gel after twice the gelling time.[28]

B. Pure silica xerogels

Figure 4 shows the $I(Q)$ measured for pure silica xerogels (a) before and (b) after heat treatment at 600 °C. Both xerogel samples show strong Q^{-n} scattering at low Q, i.e., $Q < 0.1$ Å^{-1}, which is expected due to the surfaces of xerogel powder particles [see Sec. II. B and Fig. 1(a)]. The measured $n = 2.85 \pm 0.10$ is much less than the expected value of 4.0 because of strong slit-smearing for a camera length of 1.5 m (see Sec. II. C). This effect was confirmed using reference samples with smooth particle surfaces which gave measured $n = 3.0 \pm 0.1$ compared to the expected value of 4.0. The SAXS data extends up to $Q = 0.5$ Å^{-1} and appears to show a downturn in $I(Q)$ beginning at $Q \approx 0.4$ Å^{-1}. Although the SAXS data do not extend to high enough Q to confirm the downward trend, the WAXS of silica sols[29] and titania–silica xerogels[6] shows that $I(Q)$ is strongly decreasing in the region $0.5 \leq Q \leq 0.9$ Å^{-1}. In the intermediate region, i.e., $0.1 < Q < 0.4$ Å^{-1}, there is a plateau in $I(Q)$. This feature corresponds with inhomogeneities due to micropores, as discussed in Secs. II. B and IV. B [see Fig. 1(b)]. A SAXS study of $(ZrO_2)_{0.3}(SiO_2)_{0.7}$ xerogels heat treated from 100 to 500 °C[30] shows similar plateaus.

C. TiO_2–SiO_2 xerogels

Figures 5–7 show $I(Q)$ for $(TiO_2)_x(SiO_2)_{1-x}$ xerogels with $x = 0.08$ and 0.18 and 0.41 respectively, and with heat treatment at different temperatures from none to

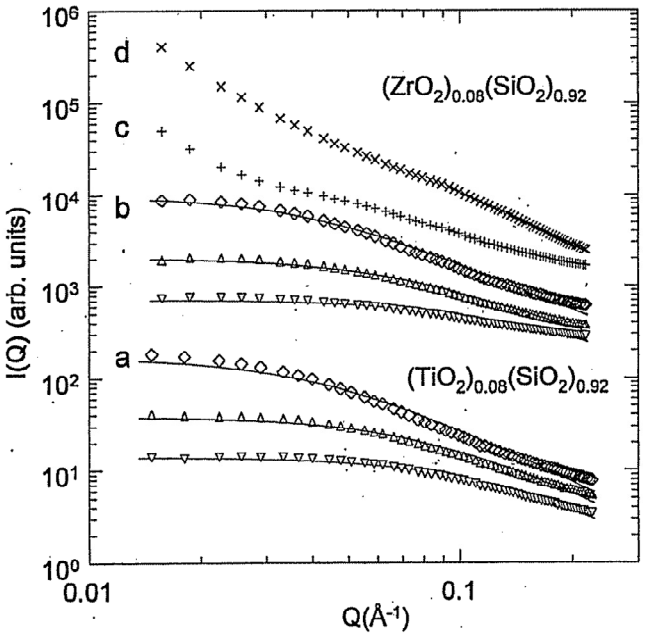

FIG. 2. $I(Q)$ for (a) $(TiO_2)_{0.08}(SiO_2)_{0.92}$ sols, (b) $(ZrO_2)_{0.07}(SiO_2)_{0.93}$ sols, and (c,d) $(ZrO_2)_{0.07}(SiO_2)_{0.93}$ gels. Sols were aged for approximately (▽) 10, (△) 200, and (◇) 700 min. Solid lines are fits (see Sec. III. A and Fig. 3). Gels were formed from sols initially aged for 720 min and then heated at 50 °C for (c) 240 and (d) 720 min. (Vertical offsets have been used. Only 30% of data points are shown.)

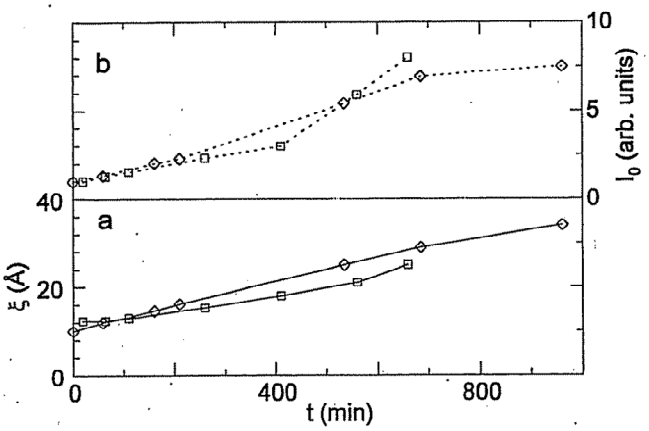

FIG. 3. Characteristic length scale of fluctuations, ξ, and intensities, I_0, obtained by fitting Ornstein–Zernike equation [Eq. (1)] to $I(Q)$ for (◇) $(TiO_2)_{0.08}(SiO_2)_{0.92}$ and (□) $(ZrO_2)_{0.07}(SiO_2)_{0.93}$ sols (see Fig. 2).

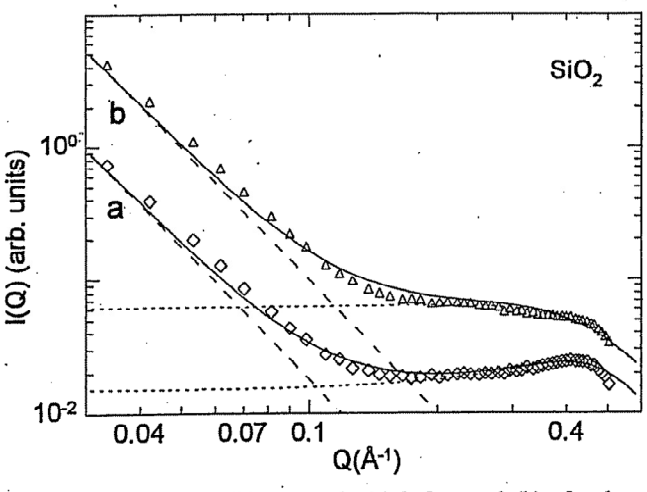

FIG. 4. $I(Q)$ for pure SiO_2 xerogels (a) before and (b) after heat treatment at 600 °C. Solid lines are fits (see Secs. III. B and IV. B). (Vertical offsets have been used. Only 30% of data points are shown.)

1000 °C. The $I(Q)$ have been offset for clarity, and the actual intensities are shown in Table I. The observation of trends in $I(Q)$ is limited due to uncertainties in normalization, which are probably due to nonuniform thickness of powder samples. However there appears to be a tendency for $I(Q)$ to increase with heat treatment which would be consistent with the densification known to occur with heat treatment.[6]

Previous studies (e.g., Ref. 16) showed that $(TiO_2)_x(SiO_2)_{1-x}$ xerogels with $x = 0.08$ have very little phase separation. Hence the $I(Q)$ for these samples (see Fig. 5) are expected to show the same features as the pure silica samples (see Fig. 4). This is indeed the case. Similar to pure silica samples, there is strong Q^{-n} scattering at low Q due to the surfaces of xerogel powder particles. The measured values of n are shown in Table I, and the average value is 3.35 ± 0.05. The effect of slit-smearing was calibrated using reference samples with smooth particle surfaces which gave measured $n = 3.65 \pm 0.05$ compared to expected $n = 4.0$. (Note that the effects of slit-smearing are much reduced for a camera length of 3.5 m compared to 1.5 m.) Also similar to pure silica xerogels, the $I(Q)$ for $x = 0.08$ xerogels have a concave shape at $Q \sim 0.1$ Å^{-1}, and this becomes less concave at higher temperatures of heat treatment. The $x = 0.18$ xerogels initially have no phase separation, but phase separation of a TiO_2 phase develops with heat treatment at ≥750 °C. In the former and latter cases the $x = 0.18$ xerogels are respectively similar to $x = 0.08$ and $x = 0.41$ xerogels (see below).

Previous studies (e.g., Refs. 14–16) showed that $(TiO_2)_{0.41}(SiO_2)_{0.59}$ xerogels have significant phase separation of TiO_2. This is apparent from OTi_n configurations observed in O^{17} NMR,[14] and from Ti–O coordinations observed in Ti K-edge extended x-ray absorption fine structure (EXAFS),[15] and is due to the limited ability of Ti to be mixed into a silica network. As discussed in Sec. II. B [see Fig. 1(c)], the presence of phase-separated regions within the silica-based network will give rise to additional scattering. Indeed, the $I(Q)$ for heat treatments at ≥250 °C show significant shoulders centered in the region of 0.05 to 0.1 Å^{-1} (see Fig. 7) relative to non-

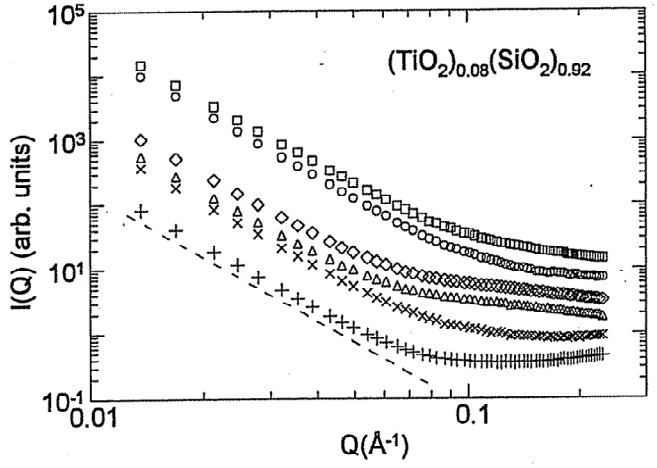

FIG. 5. $I(Q)$ for $(TiO_2)_{0.08}(SiO_2)_{0.92}$ xerogels before (+) and after heat treatment at (×) 100 °C, (△) 250 °C, (◇) 500 °C, (○) 750 °C, and (□) 1000 °C. (Vertical offsets have been used. Only 30% of data points are shown.)

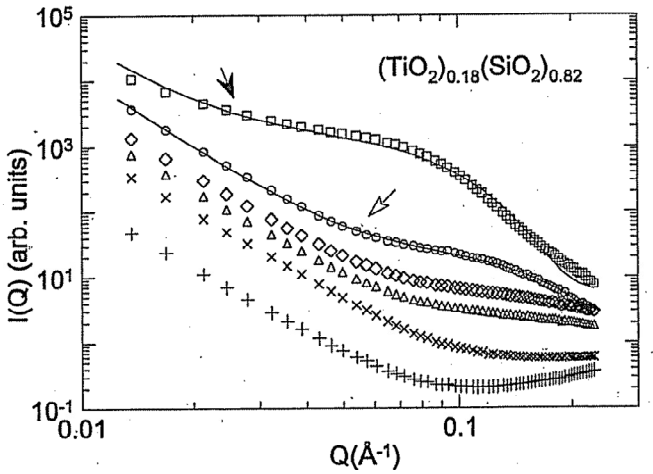

FIG. 6. $I(Q)$ for $(TiO_2)_{0.18}(SiO_2)_{0.82}$ xerogels before (+) and after heat treatment at (×) 100 °C, (△) 250 °C, (◇) 500 °C, (○) 750 °C, and (□) 1000 °C. Solid lines are fits (see Sec. III. C). Solid arrows indicate effect of crystallization. (Vertical offsets have been used. Only 30% of data points are shown.)

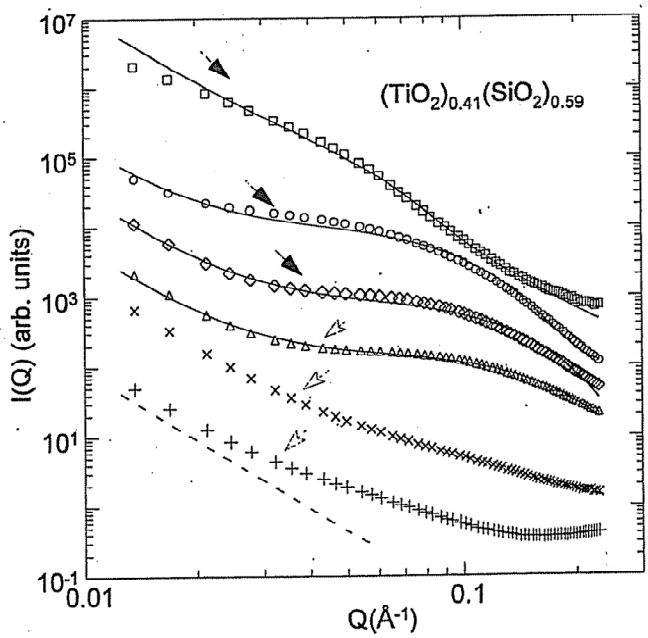

FIG. 7. $I(Q)$ for $(TiO_2)_{0.41}(SiO_2)_{0.59}$ xerogels before (+) and after heat treatment at (×) 100 °C, (△) 250 °C, (◇) 500 °C, (○) 750 °C, and (□) 1000 °C. Solid lines are fits (see Sec. III. C). Empty and solid arrows indicate effects of phase separation and crystallization (respectively). (Vertical offsets have been used. Only 30% of data points are shown.)

phase-separated samples (e.g., see Fig. 5). These features have been analyzed using the Guinier equation [Eg. (3)], with the background due to the particle surfaces represented by a term of the form Q^{-n}. To limit the number of fitted parameters a fixed value of $n = 3.35$ was used, corresponding to the mean value from Table I. The results are shown in Table II. For heat treatments at $\geq$500 °C the phase separated regions crystallize into anatase TiO_2 and can be detected by Bragg peaks in WAXS. Table II shows the crystal sizes estimated from Bragg peaks using the Scherrer equation.[31] The $I(Q)$ for heat treatments at $\leq$100 °C also show features due to phase separation, but these are difficult to analyze in the region of $Q \sim 0.1$ Å^{-1} without a more sophisticated model of the background due to the silica-based network.

TABLE I. Results of fitting $I(Q)$ of xerogels using a term of the form Q^{-n} for $Q < 0.05$ Å^{-1} (see Secs. III. C and III. D). (Note that the effects of slit-smearing were calibrated using reference samples with expected $n = 4$ which gave measured $n = 3.65 \pm 0.05$, as discussed in Sec. II. C).

Sample	Heat treatment (°C)	I_0 (arb. units) (±20%)	n (±0.05)
$(TiO_2)_x(SiO_2)_{1-x}$			
$x = 0.08$	0	0.08	3.25
	100	0.11	3.55
	250	0.14	3.35
	500	0.20	3.35
	750	0.26	3.40
	1000	0.31	3.35
$x = 0.18$	0	0.21	3.30
	100	0.19	3.35
	250	0.10	3.55
	500	0.10	3.55
	750	0.17	3.35
$x = 0.41$	0	0.11	3.05
	100	0.20	3.25
$(ZrO_2)_x(SiO_2)_{1-x}$			
$x = 0.07$	0	10.9	3.30
$x = 0.23$	0	8.3	3.15

TABLE II. Results of fitting $I(Q)$ of xerogels using the Guinier equation (Eq. 3), with low-Q background represented by a term of the form $Q^{-3.35}$ (see Secs. III. C and III. D).

		Guinier equation			
Sample	Heat treatment (°C)	I_0 (arb. units) (±20%)	diameter (Å) (±5)	R_G (Å) (±2)	WAXS diameter (Å)
$(TiO_2)_x(SiO_2)_{1-x}$					
$x = 0.18$	750	1.0	32	12	...
	1000	38	66	24	88 (±10%)
$x = 0.41$	100	6.5	28	11	...
	250	7.6	36	14	...
	500	9.1	41	16	45 (±6%)
	750	18.8	52	20	61 (±8%)
	1000	48	100	39	132 (±16%)
$(ZrO_2)_x(SiO_2)_{1-x}$					
$x = 0.32$	0	108	18	7	...
	750	293	26	9	24 (5%)

D. ZrO_2–SiO_2 xerogels

Figure 8 shows $I(Q)$ for $(ZrO_2)_x(SiO_2)_{1-x}$ xerogels with $x = 0.07$, 0.23, and 0.32 before heat treatment and for $x = 0.32$ after heat treatment at 750 °C. Although this is a limited set of results, it does show the same trends as for titania–silica xerogels. The $(ZrO_2)_x(SiO_2)_{1-x}$ xerogel with $x = 0.07$ has an $I(Q)$ similar to that for pure silica which is consistent with previous studies (e.g., Ref. 11) that showed there is very little phase separation for $x = 0.07$. There is strong Q^{-n} scattering at low Q, with a measured $n = 3.25 \pm 0.10$ (see Table I). A SAXS study of a $(ZrO_2)_{0.3}(SiO_2)_{0.7}$ xerogel[30] showed similar Q^{-n} scattering at low Q, with $n = 3.2 \pm 0.1$.

Previous studies (e.g., Ref. 11) showed that xerogels with $x = 0.23$ and $x = 0.32$ have significant phase separation of ZrO_2. This is apparent from OZr_n configurations observed in O^{17} NMR, and Zr–O coordinations observed in Zr K-edge EXAFS,[11] and is due to the limited ability of Zr to be mixed into a silica network. Indeed, the $I(Q)$ for $x = 0.23$ and $x = 0.32$ [see Figs 8(b) and 8(c)] show additional scattering in the region of $0.05 < Q \leq 0.1$ Å^{-1} relative to that for $x = 0.07$ [see Fig. 8(a)]. This additional scattering has not been analyzed for the unheated xerogels due to the difficulty of accurately fitting the background in the region of $Q \sim 0.1$ Å^{-1} due to the silica-based network. The $x = 0.32$ xerogel heated at 750 °C shows a strong shoulder centred at $Q \sim 0.1$ Å^{-1} which has been fitted using the Guinier equation (Eq. 3; see Table II). The background due to the particle surfaces was represented using a term of the form Q^{-n} with fixed

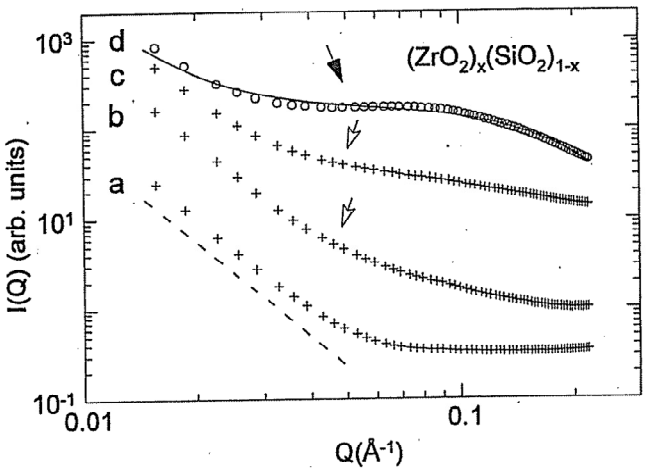

FIG. 8. $I(Q)$ for $(ZrO_2)_x(SiO_2)_{1-x}$ xerogels with (a) $x = 0.07$, (b) $x = 0.23$, and (c) $x = 0.32$, before (+) and after heat treatment at (O) 750 °C. Solid lines are fits (see Sec. III. D). Empty and solid arrows indicate effects of phase separation and crystallization. (Vertical offsets have been used. Only 30% of data points are shown.)

$n = 3.35$ (corresponding to the mean value from Table I). The WAXS results show that the $x = 0.32$ xerogel heated at 750 °C contains tetragonal ZrO_2 crystals, and Table II shows the crystal size estimated from Bragg peaks using the Scherrer equation.[31]

IV. DISCUSSION

A. Sols

In acid-catalyzed sols, hydrolysis, and condensation reactions lead to the formation of weakly branched polymeric clusters, which grow by aggregation.[5] The sizes of clusters depend on preparation conditions and are characterized by ξ [see Eq. (1)] or, equivalently for low, Q, $R_G \approx 1.73\ \xi$ [see Eq. (3)]. The values of ξ observed here are consistent with values of ξ and R_G reported for acid-catalyzed pure silica,[21,29,32,33] titania–silica,[22] and zirconia–silica[23] sols with $1 \leq R_W \leq 5$. For a cluster–cluster aggregation process the aggregate structure is predicted to be a mass fractal, with fractal dimension $1.7 \leq d_m \leq 2.1$.[28,32] In the literature, the fractal dimension is commonly estimated by fitting a Q^{-n} term in the intermediate Q-range, e.g., $0.05\ Å^{-1} < Q \leq 0.2\ Å$ (e.g., Refs. 20 and 21). However, this is not rigorous because a Q-range of at least one decade is necessary. The fractal dimension can be estimated by observing the effects of dilution on a sample.[33] It can also be determined from the values of I_0, which scale as ξ^{d_m},[22] i.e., a log–log plot of I_0 against ξ has a slope of d_m. In this way the results in Fig. 3 provide rough estimates of d_m. The observed values of 1.7 ± 0.2 and 2.5 ± 0.2 for $(TiO_2)_{0.08}(SiO_2)_{0.92}$ and $(ZrO_2)_{0.07}(SiO_2)_{0.93}$ sols, respectively, are comparable to those reported for similar sols.[21–23,29,32,33]

B. Xerogels

Here we discuss the xerogel results in relation to the three types of inhomogeneities discussed in Sec. II. B (see Fig. 1). Note that the acid-catalyzed xerogels studied here do not contain colloidal particles or aggregates as in base-catalyzed xerogels and do not contain mesopores as in aerogels.[5]

All the non-phase-separated titania– and zirconia–silica xerogel samples show strong Q^{-n} scattering at low Q, and this scattering is also evident for the samples containing phase-separated metal oxide. Here Q^{-n} is intended as a descriptive term. Our data do not extend to low enough Q values to rigorously establish Q^{-n} behavior. However, it is clear that the low-Q behavior of $I(Q)$ does not follow Porod scattering expected for smooth, sharp xerogel powder particle surfaces (i.e., expected $n = 4$). The particle surfaces are rough because they are the product of micropore perforation and fracture [see Fig. 1(a)]. The Q^{-n} behavior, and hence surface roughness, is unaffected by heat treatment up to 1000 °C. The comparison between the average n for the xerogels, i.e., 3.35 ± 0.05, and reference samples with Porod scattering, i.e., 3.65 ± 0.05, provides some measure of the roughness. If a fractal description was applied, the observed results would indicate particles with fractal surface dimension of $d_s = 2.3 \pm 0.1$. Such surface roughness has been observed for particle surfaces in clay minerals.[25] Computer simulations of fracture of porous silica have given $d_s = 2.3 \pm 0.2$.[34]

All the non-phase-separated $(TiO_2)_x(SiO_2)_{1-x}$ xerogel samples show $I(Q)$ which is concave in the region of $Q \sim 0.1\ Å^{-1}$ (see Figs. 5–7), and this corresponds to the a plateau in the region from $0.1 < Q < 0.4\ Å^{-1}$ for pure silica xerogels (see Fig. 4). These features correspond with the smallest scale inhomogeneities in the xerogels which are due to micropores in the silica-based network [see Fig. 1(b)]. As an approximation, the plateau regions in Fig. 4 have been fitted using an expression for scattering from a two-phase, bicontinuous structure with sharp boundaries,[35,36]

$$I(Q) \propto \frac{1}{(1 + aQ^2 + b^2Q^4)} \quad . \tag{6}$$

The characteristic length for persistence within a phase is $\xi = (b/2 + a/4)^{-0.5}$, and the characteristic distance between two neighboring regions of the same phase is $d = 2\pi(b/2 - a/4)^{-0.5}$. The degree of correlation between the two phases is indicated by the strength of the peak at $Q \sim 2\pi/d$ (note that $d = 0$ for a random mixture).

The results of fitting Eq. (6) to the $I(Q)$ for pure silica xerogels are shown in Fig. 4. The parameters obtained for samples (a) before and (b) after heat treatment at 600 °C were (a) $\xi = 0.9 \pm 0.2$ Å and $d = 11 \pm 3$ Å and (b) $\xi = 1.5 \pm 0.2$ Å and $d = 8 \pm 2$ Å, respectively. These values are in the range expected for inhomogeneities on the scale of 5 to 10 Å corresponding to micropores (ξ is approximately comparable to $0.6R_G$ or 0.2 × diameter). The $I(Q)$ for the unheated sample shows evidence of a peak at $0.45\ Å^{-1}$, but heat treatment causes this part of the plateau to become diminished. Heat treatment of xerogels causes Oswald ripening,[5] in which surface tension is minimised by reducing the curvature of the boundary between the silica-based network and micropores.

As discusssed above, the $I(Q)$ for all the xerogel samples is dominated at low and high Q by the contributions from rough particle surfaces and from micropores respectively (e.g., see Figs. 4 and 5). In comparison, the $I(Q)$ for heat-treated $(TiO_2)_{0.41}(SiO_2)_{0.58}$ and $(ZrO_2)_{0.32}(SiO_2)_{0.68}$ xerogels (see Figs. 7 and 8) have large shoulders centered in the region of $0.05 < Q \leq 0.1\ Å^{-1}$. These features correspond to phase separation in the form of crystallization of metal oxides, as confirmed by simultaneous WAXS measurements. They have been modeled using the Gunier equation [Eq. (3)] plus a $Q^{-3.35}$

term to account for the effects of rough particle surfaces. Although this modeling is crude, because the Guinier equation assumes a single object size and is not rigorous for $QR_G > 1$, the values of R_G obtained are in good agreement with the estimates of crystal sizes from WAXS measurements (see Table II). More interestingly, the same features are seen with $I(Q)$ for $(TiO_2)_{0.41}(SiO_2)_{0.58}$ and $(ZrO_2)_{0.32}(SiO_2)_{0.68}$ xerogels prior to crystallization. Hence SAXS shows the presence of phase separated regions of amorphous metal oxide. The $(TiO_2)_{0.18}(SiO_2)_{0.82}$ xerogel is initially non-phase-separated, and phase separation of TiO_2 occurs because heat treatment reduces the solubility of Ti in the silica network, as suggested by our previous work.[16]

V. CONCLUSIONS

The SAXS results presented here for acid-catalyzed titania–silica and zirconia–silica sols and xerogels have been interpreted in terms of the known structural features of these materials.[5] *In situ* SAXS of $(TiO_2)_{0.08}(SiO_2)_{0.92}$ and $(ZrO_2)_{0.07}(SiO_2)_{0.93}$ sols during aging shows the growth of polymeric clusters with characteristic length scale of ~20 Å. For $(TiO_2)_x(SiO_2)_{1-x}$ and $(ZrO_2)_x(SiO_2)_{1-x}$ xerogels with $x < 0.1$ there is no phase separation (e.g., Refs. 11 and 16), but the SAXS results show the presence of two types of inhomogeneity. For $Q < 0.05$ Å^{-1} there is a clear departure from Porod scattering which shows that xerogel powder particle surfaces are rough. For $0.1 < Q < 0.4$ Å^{-1} there is a plateau feature corresponding to micropores within the silica-based network. For $(TiO_2)_x(SiO_2)_{1-x}$ and $(ZrO_2)_x(SiO_2)_{1-x}$ xerogels with $x \geq 0.2$ heat treatment causes phase separation and eventual crystallization of metal oxide. The SAXS results clearly show the presence of phase-separated regions of amorphous metal oxide in unheated xerogels with $x > 0.3$. The $(TiO_2)_{0.18}(SiO_2)_{0.82}$ xerogels are not phase separated before heat treatment but become so after heat treatment at 750 °C due to reduced solubility of Ti in the silica network.

ACKNOWLEDGMENTS

We wish to thank B.U. Komanschek for help with experiments, D.M. Pickup and J.C. Dore for helpful discussions, and the Engineering and Physical Sciences Research Council (EPSRC) and Central Laboratory of the Research Councils (CCLRC) for funding this work through various grants.

REFERENCES

1. P.C. Shultz and H.T. Smyth, in *Amorphous Materials,* edited by E.W. Douglas and B. Ellis (Wiley, London, United Kingdom, 1972).
2. M. Itoh, H. Hattori, and K.J. Tanabe, J. Catal. **35,** 225 (1974).
3. M. Nogami, J. Non-Cryst. Solids **69,** 415 (1985).
4. J.B. Miller and E.I. Ko, J. Catal. **159,** 58 (1996).
5. C.J. Brinker and G.W. Scherer, *Sol-Gel Science* (Academic Press, San Diego, CA, 1990).
6. J.S. Rigden, R.J. Newport, M.E. Smith, P.J. Dirken, and G. Bushnell-Wye, J Mater. Chem. **6,** 337 (1996).
7. J.K. Walters, J.S. Rigden, P.J. Dirken, M.E. Smith, W.S. Howells, and R.J. Newport, Chem. Phys. Lett. **264,** 539 (1997).
8. M. Emili, L. Incoccia, S. Mobilio, G. Fagherazzi, and M. Guglielmi, J. Non-Cryst. Solids **74,** 129 (1985).
9. O. Stachs, T. Gerber, and V. Petkov, J. Mater. Sci. **32,** 4209 (1997).
10. Z. Liu and R.J. Davis, J. Phys. Chem. **98,** 1253 (1994).
11. D.M. Pickup, G. Mountjoy, G.W. Wallidge, R.J. Newport, and M.E. Smith, Phys. Chem. Chem. Phys. **1,** 2527 (1999).
12. K.L. Walther, A. Wokaun, B.E. Handy, and A. Baiker, J. Non-Cryst. Solids **134,** 47 (1991).
13. S.W. Lee and R.A. Condrate, J. Mater. Sci. **23,** 2951 (1988).
14. P.J. Dirken, M.E. Smith, and H.J. Whitfield, J. Phys. Chem. **99,** 395 (1995).
15. R. Anderson, G. Mountjoy, R.J. Newport, and M.E. Smith, J. Non-Cryst. Solids **232–234,** 72 (1998).
16. G. Mountjoy, D.M. Pickup, G.W. Wallidge, R. Anderson, J.M. Cole, R.J. Newport, and M.E. Smith, Chem. Mater. **11,** 1253 (1999).
17. K. Okasaka, H. Nasu, and K. Kamiya, J. Non-Cryst. Solids **136,** 103 (1991).
18. L.A. Feigin and D.I. Svergun, *Structure Analysis by Small-Angle X-ray and Neutron Scattering* (Plenum Press, New York, 1987).
19. I.M. Miranda Salvado, F.M.A. Margaca, and J. Teixeira, J. Non-Cryst. Solids **163,** 115 (1993).
20. F.M.A. Margaca, I.M. Miranda Salvado, and J. Teixeira, J. Non-Cryst. Solids **209,** 143 (1997).
21. T. Kamiya, M. Mikami, and K. Suzuki, J. Non-Cryst. Solids **150,** 157 (1992).
22. M. Ramirez-del-Solar, L. Esquivias, A.F. Craievich, and J. Zarzycki, J. Non-Cryst. Solids **147–148,** 206 (1992).
23. M. Nogami and K. Nagasaka, J. Non-Cryst. Solids **109,** 79 (1989).
24. B.E. Yoldas, J. Non-Cryst. Solids **38–39,** 81 (1980).
25. P.W. Schmidt, J. Appl. Crystallogr. **24,** 414 (1991).
26. S.K. Sinha, E.B. Sirota, and S. Garoff, Phys. Rev. B **38,** 2297 (1988).
27. O. Glatter and O. Kratky, *Small Angle X-ray Scattering* (Academic Press, London, United Kingdom, 1982), p. 121.
28. O. Stachs, T. Gerber, Y. Beyer, and H. Burger, J. Non-Cryst. Solids **180,** 197 (1995).
29. B. Himmel, T. Gerber, and H. Burger, J. Non-Cryst. Solids **119,** 1 (1990).
30. O. Stachs, V. Petkov, and T. Gerber, J. Appl. Crystallogr. **30,** 670 (1997).
31. B.E. Warren, *X-ray Diffraction* (Addison-Wesley, Reading, United Kingdom, 1969), p. 253.
32. B.N. Nair, W.J. Elferink, K. Keizer, and H. Verweij, J. Colloid Interface Sci. **178,** 565 (1996).
33. D.W. Schaefer and K.D. Keefer, Phys. Rev. Lett. **53,** 1383 (1984).
34. A. Nakano, R.K. Kalia, and P. Vashishta, Phys. Rev. Lett. **73,** 2336 (1994).
35. M. Teubner and R. Strey, J. Chem. Phys. **87,** 3195 (1987).
36. J.-C. Li and D.K. Ross, J. Phys.: Condens. Matter **6,** 351 (1994).